Colloids and Surfaces A: Physicochem. Eng. Aspects 506 (2016) 344–355

Contents lists available at ScienceDirect

Colloids and Surfaces A: Physicochemical and Engineering Aspects

journal homepage: www.elsevier.com/locate/colsurfa

Smart water channelling through dual wettability by leaves of the bamboo *Phyllostachys aurea*

J.M. Wigzell[a], R.C. Racovita[b], B.G. Stentiford[a], M. Wilson[a], M.T. Harris[a], I.W. Fletcher[c], D.P.K. Mosquin[d], D. Justice[d], S.K. Beaumont[a], R. Jetter[b,e,1], J.P.S. Badyal[a,*,1]

[a] Department of Chemistry, Science Laboratories, Durham University, Durham DH1 3LE, England, UK
[b] Department of Chemistry, University of British Columbia, Vancouver, V6T 1Z1, Canada
[c] School of Mechanical and Systems Engineering, Newcastle University, Newcastle NE1 7RU, UK
[d] UBC Botanical Garden, University of British Columbia, Vancouver, V6T 1Z4, Canada
[e] Department of Botany, University of British Columbia, Vancouver, V6T 1Z4, Canada

HIGHLIGHTS

- Dual hydrophobic-hydrophilic wettability of young *Phyllostachys aurea* bamboo leaf surfaces leads to water channelling and self-cleaning.
- Nanoscale roughness of epicuticular waxes combined with very-long-chain alkyl compounds underpin localised leaf wetting characteristics.
- Bioinspired replication of such dual wetting may offer potential for fog collection and dew harvesting in water-scarce regions of the world.

GRAPHICAL ABSTRACT

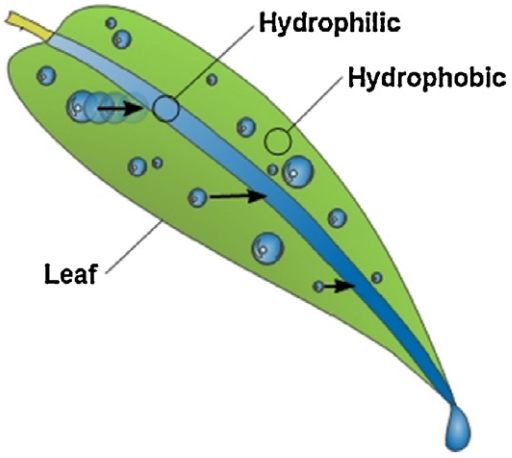

ARTICLE INFO

Article history:
Received 10 May 2016
Received in revised form 26 June 2016
Accepted 28 June 2016
Available online 29 June 2016

Keywords:
Water harvesting
Dual surface wetting
Bamboo
Bioinspired

ABSTRACT

The young leaves of the bamboo plant, *Phyllostachys aurea*, exhibit a distinct dual wetting behaviour on their adaxial surface. Contact angle analysis, variable pressure (environmental) scanning electron microscopy, gas chromatography, time-of-flight secondary ion mass spectrometry, and X-ray photoelectron spectroscopy have shown that the epicuticular wax morphology/topography and the surface distribution of chemical species underpin this water-channelling behaviour. Envisaged bioinspired applications include fog and dew harvesting in water-scarce regions of the world.

1. Introduction

The study of plant surfaces [1–3], has led to the discovery of some fascinating phenomena including the superhydrophobicity of *Nelumbo nucifera* (Indian lotus) leaf [4], water adhesion on *Rosa*

* Corresponding author.
E-mail address: j.p.badyal@durham.ac.uk (J.P.S. Badyal).
[1] These authors have made equal contributions.

http://dx.doi.org/10.1016/j.colsurfa.2016.06.058

moyesii (red rose) [5], dry adhesion by *Galium aparine* [6], fog harvesting by *Cotula fallax* [7], and water channelling by *Thuja plicata* [8]. The understanding and replication of such surfaces is paving the way to many everyday technological applications; for example, self-cleaning designs based upon the lotus leaf have been introduced into the paint, glass, automotive, and textile industries [9]. Plant species displaying a range of wettabilities have been widely studied [10,11]. These have included different wettabilities on opposite sides of the same leaf [12], as well at different stages of leaf growth [13,14]. Quite often, these properties can be related to the native environment of the plants, as for instance in the case of the Namib Desert grass, *Stipagrostis sabulicola*, whose leaves collect water from mist in lieu of uptake from soil [15]. Despite the number of plant surfaces studied, the range of wetting phenomena reported has been fairly limited (such as hydrophobicity, hydrophilicity, and fog capture) [16,17].

The present study focuses on the unusual dual wetting behaviour of the young leaves of *Phyllostachys aurea*, a bamboo that originates in East Asia. In order to further understand this mechanism, the physical and chemical properties of these surfaces have been compared between young and old leaves using contact angle analysis, (environmental) scanning electron microscopy, gas chromatography, time-of-flight secondary ion mass spectrometry, and X-ray photoelectron spectroscopy.

2. Experimental

2.1. *Preparation of* Phyllostachys aurea *samples*

Phyllostachys aurea plant cuttings were collected from outdoor beds, situated in Northern England and Western Canada climates (both temperate oceanic climates), and their stems kept in water to minimize dehydration during transportation to nearby analytical facilities.

2.2. *Contact angle measurements*

Contact angles were measured at room temperature using a video capture apparatus (VCA 2500 XE, AST Products Inc.) and 1 μL high-purity water droplets (ISO 3696 grade 1). Static water contact angle values less than 90° signify a hydrophilic surface, whilst greater than 90° corresponds to a hydrophobic surface [18]. Advancing and receding contact angle values were determined by respectively increasing or decreasing the liquid drop volume [19].

2.3. *Variable pressure (environmental) scanning electron microscopy (ESEM)*

An environmental scanning electron microscope (XL30 ESEM-FEG, FEI Company) operating in wet mode was used to monitor water vapor condensation onto individual leaf samples in real time. The leaves were mounted onto carbon disks and attached to a Peltier cooling stage. Vapor condensation was controlled by varying the chamber pressure and sample temperature. Electron micrographs were taken using a gaseous secondary electron detector (GSED), in conjunction with a 15 kV accelerating voltage, and a working distance between 9 and 11 mm.

2.4. *Scanning electron microscopy (SEM)*

Individual leaf specimens were prepared for scanning electron microscopy analysis by using a glycerol substitution process [20]. Each sample was then mounted onto a carbon disk. No gold coating was required due to the conductive nature of the glycerol [21]. Plant surface structure images were taken on a scanning electron microscope (Stereoscan 240, Cambridge Instruments Company) operating in a secondary electron detection mode, in conjunction with an 8 kV accelerating voltage, and a working distance between 9 and 35 mm.

2.5. *Gas chromatography (GC)*

2.5.1. *Extraction of adaxial leaf wax*

To selectively extract cuticular wax only from the adaxial side of the leaf, one end of a glass cylinder (Schott, Standard expansion adapter NSE 19/14, open at both ends) was gently pressed onto the leaf surface with sufficient force to create a seal between cylinder and leaf whilst not damaging the plant material, and filled three times with 1.5 mL of fresh chloroform (Aldrich, ≥99%, 0.75% ethanol as stabilizer) at room temperature, with intermittent agitation of the chloroform using a Pasteur pipette. The chloroform extracts from five randomly chosen leaf surface areas were combined, concentrated at 50 °C under a stream of N_2 (Praxair, ≥99.998%), and stored prior to analysis. The total surface area per sample was calculated from the diameter of the cylinder to be 3.6 cm^2 [13].

2.5.2. *Analysis of wax extracts*

Before GC–MS/FID analysis, wax extracts were spiked with 10 μL of a 1.02 mg/mL solution of *n*-tetracosane (Alfa Aesar, ≥99%) in chloroform as an internal standard and subjected to derivatization with 10 μL of *N,O*-bis(trimethylsilyl)trifluoroacetamide (BSTFA, Aldrich, GC grade) in 10 μL pyridine (Aldrich, ≥99.8%, anhydrous) for 30 min at 70 °C. Then, they were concentrated to dryness at 50 °C under a stream of N_2 and re-dissolved in 20 μL chloroform to a total volume of 20 μL. Under these conditions, amides did not undergo silylation, resulting in poor chromatographic peak shape for these wax constituents. Therefore, after re-evaporation to dryness, samples were derivatized for 1 h at 70 °C in 20 μL of benzyl bromide (Aldrich, ≥98%) in the presence of 0.1 mg NaH (Aldrich, anhydrous, ≥95%). Then, excess NaH was quenched with distilled water, the basic aqueous layer discarded and the organic layer containing benzylated derivatives taken to dryness. Finally, the resulting mixture was again subjected to silylation with BSTFA/pyridine as described above, dried, and brought to a final volume of 20 μL with fresh chloroform.

Two different GC instruments were used for separation and detection of wax constituents, both equipped with the same type of capillary GC column (6890N, Agilent, Avondale PA, USA; 30 m long; type HP-1: 100% PDMS; 0.32 mm i.d.; df = 0.1 μm) and following the same temperature program (on-column injection at 50 °C, constant for 2 min, ramp 40 °C min^{-1} to 200 °C, constant for 2 min, ramp 3 °C min^{-1} to 320 °C, constant for 30 min). The first instrument employed He gas (Praxair, ≥99%) as the mobile phase, at a flow rate of 1.4 mL min^{-1}, and was equipped with an MS detector (5973N, Agilent, EI-70 eV), primarily serving the purpose of qualitative identification of the separated wax compounds. The second instrument used H_2 carrier gas (Praxair, ≥99.95%) at 2.0 mL min^{-1} and an FID detector for the quantification of individual wax homologs/isomers, based on normalization of their peak areas against that of the internal standard. It had been shown previously that most wax compounds have relative response factors of 1.00 to this standard under very similar GC-FID conditions [22]. Quantitative compositions of aliphatic ester metamers were determined from GC–MS data as described by Lai et al. [23].

2.6. *Time-of-Flight secondary ion mass spectrometry (ToF-SIMS)*

The leaf samples for ToF-SIMS analysis were mounted onto a piece of double-sided tape (3M 'Scotch Tape', grade 665) attached to a piece of clean PET film (Melinex, 'O' grade). A second piece of PET film, containing a square hole in the centre, was mounted over the leaf in an attempt to minimize the tendency for the leaf

margins to curl over. This assembly was attached to the base plate of a sample holder using stainless steel clips.

Static SIMS analysis was carried out using an instrument of single-stage reflectron design (TOF-SIMS IV – 200, ION-TOF GmbH) [24]. Positive and negative ion mass spectra and images of the leaf samples were obtained using a 20 keV Bi_3^{2+} focused liquid metal ion beam, incident at 45° to the surface normal, and operated in 'bunched' mode for high mass resolution (20 ns wide ion pulses at a 6.7 kHz repetition rate). Charge compensation was provided by a low-energy (ca. 20 eV) electron flood gun. The total ion dose density was kept to less than 1×10^{16} ions m^{-2} in all cases. Sample surface topography and the ion gun mode of operation limited the mass resolution to ca. $m/\Delta m = 1000$. Positive and negative ion static SIMS spectra of the samples were recorded at room temperature with a 128×128 pixel raster and a field of view of $200\,\mu m \times 200\,\mu m$, and the sample imaged with a field of view of $500\,\mu m \times 500\,\mu m$. In addition, images and spectra were recorded from larger areas in the range $7\,mm \times 7\,mm$ up to $12.5\,mm \times 12.5\,mm$ by moving the sample under the ion beam (the so-called 'stage raster' mode of operation).

2.7. X-Ray photoelectron spectroscopy (XPS)

X-ray Photoelectron Spectroscopy (XPS) surface characterization was carried out using an electron spectrometer (AXIS Nova, Kratos Analytical Ltd), equipped with a monochromated Al Kα X-ray source (1486.6 eV) and a concentric hemispherical analyser combined with a spherical mirror analyser. Photoelectrons were collected at a take-off angle of 0° from the substrate normal (mean escape depth = ~0.5–1.5 nm) [25], with electron detection in the constant analyser energy mode (CAE mode, pass energy = 160 eV for wide scan & 20 eV for high resolution spectra, step size = 1.0 eV & 0.1 eV, respectively). Rectangular samples, spanning the width of the leaf, were cut from fresh *Phyllostachys aurea* leaves and mounted, adaxial side facing upwards, onto an aluminum sample plate. Beryllium-copper clips were used to secure the samples. The leaves were preloaded into the system at a pressure of 10^{-7} mbar for 2–3 h, and then transferred into the XPS analysis chamber at 10^{-8} mbar. For all elements detected in the XPS survey spectrum, elemental compositions were calculated using experimentally determined machine-specific sensitivity factors, based on the Wagner values [26]: C(1s): O(1s): N(1s): Si(2p) equals 1.00: 2.81: 1.72: 1.18. The C(1s) core level binding energy envelopes were fitted using a Gaussian peak shape for the -$\underline{C}_xH_y$ hydrocarbon component and a linear background [27,28]. All binding energies were referenced to the C(1s) -$\underline{C}_xH_y$ hydrocarbon peak at 285.0 eV [29]. Fitted component peak FWHM values used were comparable to those obtained using a low-density polyethylene reference sample analysed on the same instrument under similar conditions. Two sets of young and old *P.aurea* leaf pairs were harvested over a period of two months (July–August 2014) for analysis. The adaxial leaf surfaces were sampled at least in three different positions for each of the margin and middle regions (24 readings in total).

3. Results

3.1. The dual wettability of Phyllostachys aurea

The *Phyllostachys aurea* leaf shape changes during the different stages of its development. Initially, the sprouted *P. aurea* leaf is rolled up in a spear-like shape, pointing upwards, and with its adaxial surface completely protected from the outside elements. As the leaf begins to unravel, the adaxial surface appears to be hydrophobic, except at the point at which the leaf joins to the petiole. The leaf surface develops its dual wettable characteristics whilst still in an upright position, and this property persists once the leaf bends towards its natural position pointing downwards, Fig. 1 and Supporting Information Fig. S 1.

The young lanceolate leaves of *Phyllostachys aurea* appear to have two distinctly different regions of wettability across their adaxial surface, Fig. 1(a–c). Water landing on the leaf margins beads up in a near-superhydrophobic fashion (contact angle greater than 140°); whilst in the middle (including the midrib), the water spreads due to the hydrophilic nature of the surface (contact angle less than 90°), Table 1. These contrasting wettabilities are most noticeable in the movement of water across the leaf surface. Once large enough, droplets of water on the margin of the leaf roll towards the middle, assisted by the low contact angle hysteresis

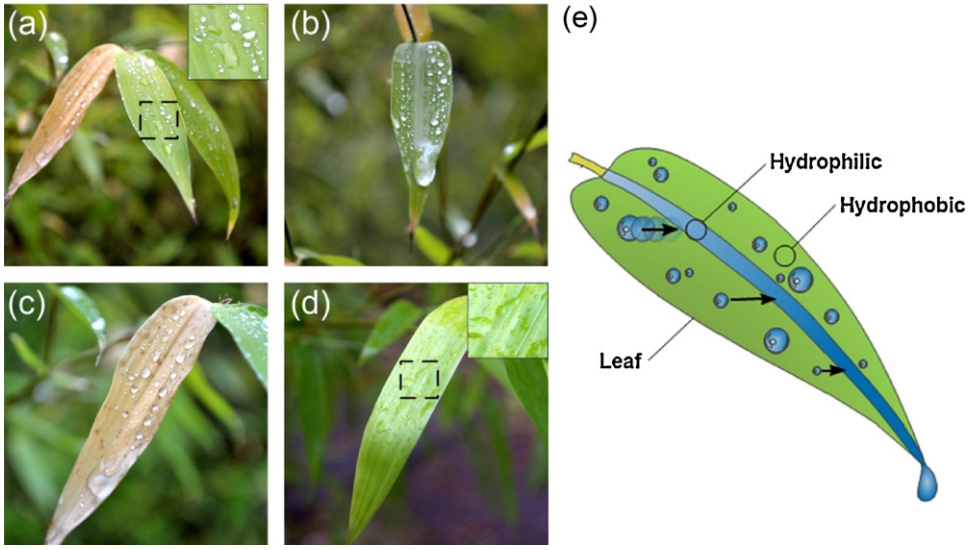

Fig. 1. Images of the adaxial surface of *Phyllostachys aurea* leaves following rainfall: (a) a young leaf exhibiting dual wettability – the combination of hydrophobic margins and a hydrophilic middle (the image in the top corner shows a magnified view of the area outlined by a dashed box); (b) a young leaf showing the results of coalescing droplets in the middle of the leaf moving downwards to the leaf tip; (c) a dead young leaf still showing the same dual wetting property; (d) an older leaf not exhibiting the dual wettability (the image in the top corner shows a magnified view of the area of the surface outlined by a dashed box); and (e) schematic illustrating dual wetting behaviour on young leaf.

Table 1
Water contact angle values for the adaxial surface of *Phyllostachys aurea* leaves.

Phyllostachys aurea Adaxial Surface	Water Contact Angle/°			
	Static	Advancing	Receding	Hysteresis
Young Leaf (Margin)	141 ± 3	142 ± 2	136 ± 4	5 ± 4
Young Leaf (Middle)	77 ± 13	84 ± 12	62 ± 10	23 ± 8
Older Leaf (Margin)	69 ± 12	83 ± 12	51 ± 11	32 ± 6
Older Leaf (Middle)	69 ± 14	87 ± 12	60 ± 10	27 ± 7

inherent to the margin, Table 1, and the slight gradient downwards due to the concave shape of the leaf, Fig. 1(a). Pools of water collecting in the middle eventually coalesce over time, forming a downward stream-like film of water, Fig. 1(b–c). As the stream increases in volume, the water flow begins to move towards the leaf tip, assisted by the hanging gradient present between the petiole and the apex of the leaf. Eventually, the droplet formed at the apex falls to the ground. In contrast, the abaxial (underside) surface of young *Phyllostachys aurea* leaves consists of a different physical structure visible to the naked eye and displays an absence of dual wetting (superhydrophobicity everywhere with water static contact angle exceeding 160°).

Interestingly, this dual wetting behaviour persists in leaves which have died early in their development but are still attached to the stem, Fig. 1(c). Furthermore, this characteristic water collection mechanism associated with the younger leaves is found to be absent for older leaves of the same species, Fig. 1(d). Their adaxial surfaces appear to be hydrophilic throughout, Table 1, and there-

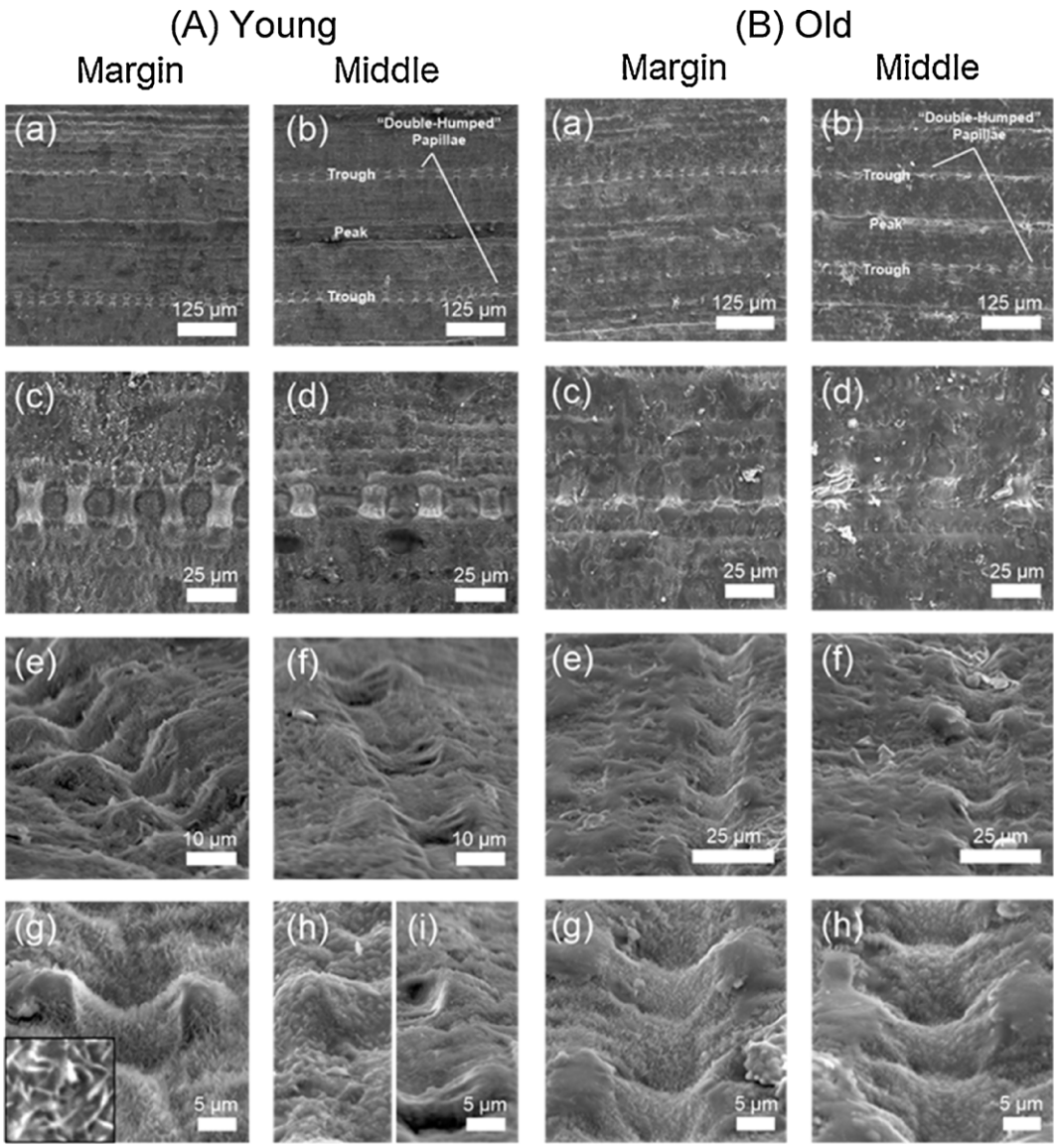

Fig. 2. SEM of the adaxial surface of (A) young and (B) old *Phyllostachys aurea* leaves. Micrographs at increasing magnifications of the: (a) margin and (b) middle of the leaf; the "double humped" papillae which make up the troughs on the: (c) margin and (d) middle; a tilted view of the "double-humped" papillae on the: (e) margin and (f) middle; and the nanoscale epicuticular wax crystals which cover the surface on the: (g) margin (inset shows the platelet-shaped wax crystals) and (h,i) middle. The horizontal axis in (a)–(d) is parallel to the leaf axis.

fore water spreads to wet both the middle and margins of these leaves.

3.2. Electron microscopy

Comparison of scanning electron microscopy (SEM) micrographs for the margin and the middle of young *Phyllostachys aurea* leaves revealed distinct differences in surface micro- and nano-scale structure, Fig. 2A. In both regions, there were perpendicularly orientated "double-humped" papillae running parallel to the macroscopic longitudinal leaf grooves between the petiole and the leaf tip. At the margin, these papillae displayed deep troughs in between their peaks as well as between the individual pairs of papillae, Fig. 2A(e). In contrast, the troughs in the middle appeared shallow and considerably less defined (lower roughness), Fig. 2A(f). These differences were further evident for the nanoscale epicuticular wax crystals covering some of the micro-relief in both areas. The surface at the margin of the leaves is covered in a dense "carpet" of upright platelet-shaped wax crystals, approximately 0.5–1 μm in height, Fig. 2A(g). In contrast, the wax crystals in the middle are granular and approximately 0.1–0.5 μm high, Fig. 2A(h–i).

Scanning Electron Microscopy (SEM) showed a smooth surface in both the margin and centre of old *Phyllostachys aurea* leaves, Fig. 2B. This appears to swamp the microscale papillae features and the majority of the nanoscale wax crystals, resulting in a much smoother surface. However, in the papillae troughs some of the features seen for the margin and middle of young leaves appear to have been retained, Fig. 2B(g–h). One noticeable difference when compared to the young leaves is the softening/suppression (lower roughness) of the nanoscale vertical-platelet wax crystals found on the leaves' margin (<0.5 μm in height on the older leaves), Fig. 2B(g).

Environmental scanning electron microscopy (ESEM) identified the characteristic wetting properties of the young *Phyllostachys aurea* leaves on a magnified scale, Fig. 3. Condensing fine water droplets appear to nucleate randomly across the surface of the margin, and in a similarly indiscriminative manner, but in larger pools across the middle.

3.3. Gas chromatography (GC)

To establish the identities and abundances of all lipids coating the adaxial side of *Phyllostachys aurea* leaves, total wax mixtures were extracted from young and old plant leaves. The waxes were identified and quantified using gas chromatography-mass spectrometry (GC–MS) and gas chromatography-flame ionization detection (GC-FID), respectively.

3.3.1. Classes of cuticular wax constituents

The total adaxial wax coverage was very similar on young and old *Phyllostachys aurea* leaves: $3.6 \pm 0.4\ \mu g\ cm^{-2}$ and $3.3 \pm 0.1\ \mu g\ cm^{-2}$, respectively. In both cases, more than 90% of the GC-detectable compounds could be identified (Fig. 4A), and cyclic terpenoids constituted almost half of the wax mixtures ($1.5 \pm 0.2\ \mu g\ cm^{-2}$ and $1.6 \pm 0.2\ \mu g\ cm^{-2}$, respectively). They were accompanied by very-long-chain (VLC) fatty acids, primary alcohols, alkyl esters, aldehydes, alkanes, and amides. Most of these compounds were present in similar amounts on young and old *P. aurea* leaves. However, free alcohols were found in higher abundance on the surface of young plants as compared to old ones ($0.30 \pm 0.04\ \mu g\ cm^{-2}$ vs. $0.18 \pm 0.01\ \mu g\ cm^{-2}$). Overall, terpenoids together with alkyl esters and fatty acids made up three quarters of the wax mixture, in a ratio of *ca.* 4:1:1, irrespective of plant age.

3.3.2. Homolog/Isomer distributions within cuticular wax classes

All VLC aliphatic classes comprised a series of homologous compounds. Alkyl esters, fatty acids, alcohols, aldehydes and amides were dominated by homologs with even carbon numbers, and alkanes by odd-numbered homologs, Fig. 4B. Generally, the chain length distributions of linear aliphatics were similar between adaxial surface waxes of young and old *Phyllostachys aurea* leaves. Free acids exhibited bimodal distributions, peaking at the C_{28} and C_{16} homologs irrespective of age, with slightly higher amounts of C_{16}, C_{18}, and C_{20} acids on old *P. aurea* leaves. The alcohol and alkane series were fairly evenly distributed, peaking at C_{28} and C_{29}, respectively, in young and old leaves alike.

Three compound classes had homolog profiles changing with age. In the aldehyde fraction, the predominant homolog (C_{30}) was accompanied by slightly more of the shorter homologs in young leaves and longer homologs in old leaves, Fig. 4B. An identical age-related chain length effect was observed for amides, also peaking at C_{30} and with shorter homologs more abundant for young and longer ones for old plant leaves. Further evidence for amide structure elucidation and related biology will be presented elsewhere [30]. Finally, the ester homolog profiles peaked at C_{48} on leaf surfaces of both ages, accompanied by near-identical amounts of the C_{46}, C_{44}, and C_{42} homologs, and higher proportions of C_{40} and C_{38} homologs on young leaves versus higher abundance of the C_{50} homolog on old leaves.

Pentacyclic triterpenoids were found in similar amounts within the wax mixtures of young and old *Phyllostachys aurea* leaves, Fig. 4B. Free triterpene alcohols dominated, with β-amyrin and isomultiflorenol together accounting for more than half of the terpenoid load. Other free triterpenols (lupeol, α-amyrin, glutinol and epifriedelanol) were less abundant. Interestingly, triterpenoid esters amounted to *ca.* 25–30% of all terpenoids, corresponding to approximately an eighth of the total adaxial wax coverage for both old and young leaves, and thus making triterpenoid and VLC alkyl esters equally abundant (compare Figs. 4A and B). Palmitates of β-amyrin, isomultiflorenol, glutinol and α-amyrin were found in a 3:3:3:1 ratio on young and old leaves alike. Additionally, trace amounts of α- and γ-tocopherols were detected, Fig. 4B.

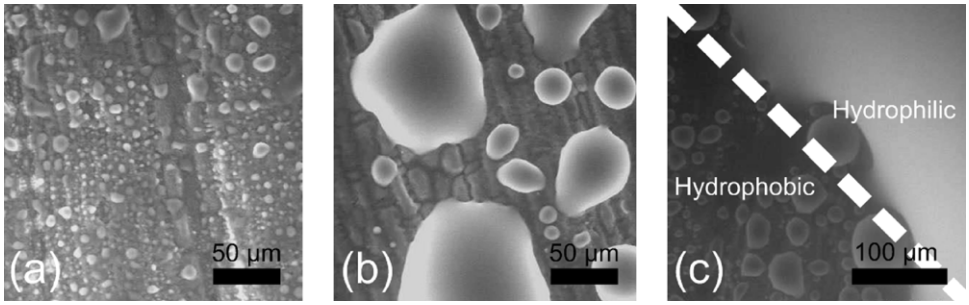

Fig. 3. ESEM micrographs of the adaxial surface of young *Phyllostachys aurea* leaves: (a) water beading on the margin; (b) water spreading in the middle; and (c) the difference in wettability at the transition zone (indicated by the dashed line) between the hydrophobic margin (lower left) and hydrophilic middle (upper right) of the leaf.

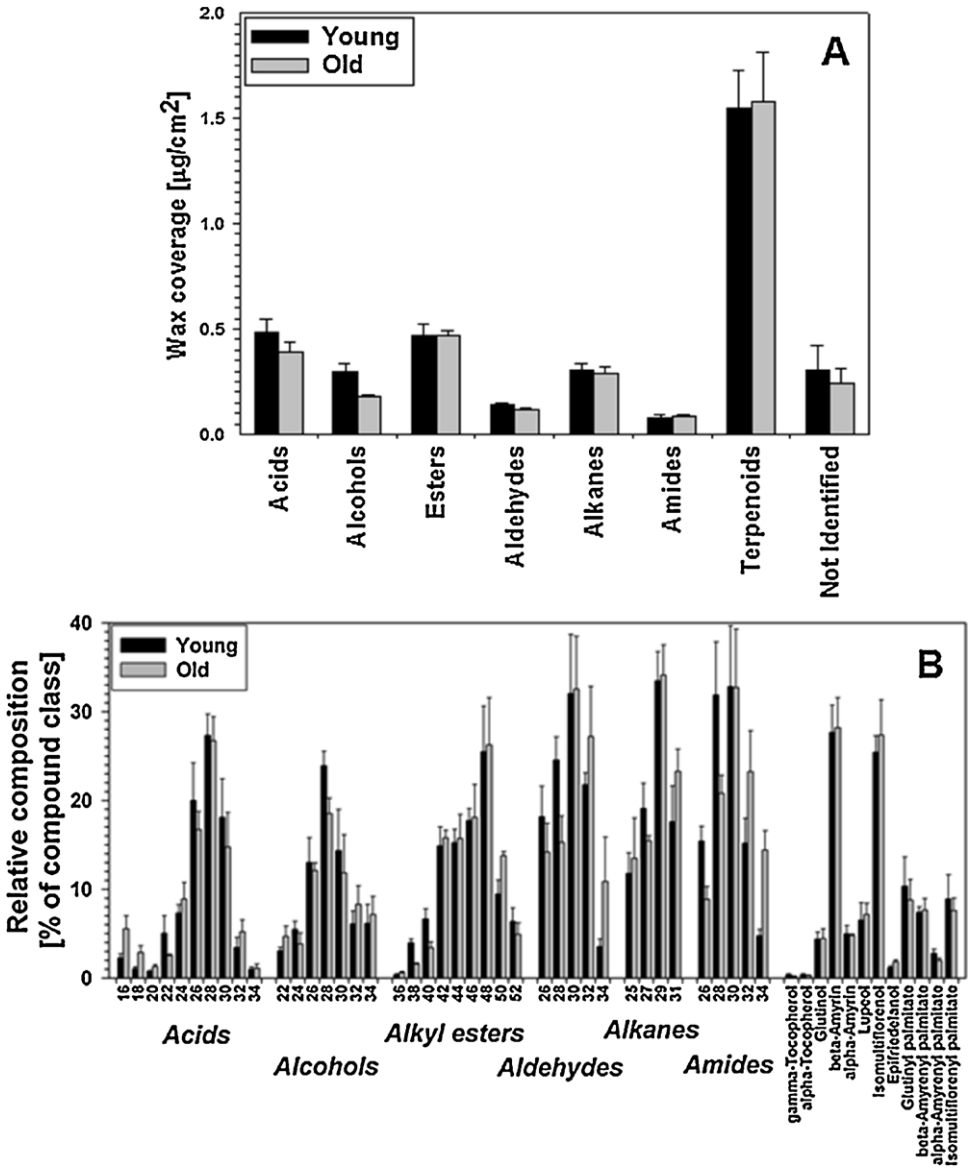

Fig. 4. (A) Compound class distribution in the wax mixtures on the adaxial side of *Phyllostachys aurea* leaves. Total coverages ($\mu g\,cm^{-2}$) of compound classes are given for the wax mixtures of young and old P. aurea leaves. (B) Relative compositions within wax compound classes within the wax mixtures on the adaxial side of *Phyllostachys aurea* leaves. Relative abundances (%) of individual homologs or isomers (in the case of terpenoids) from each compound class are given for young and old P. aurea leaves. Numbers on the x-axis indicate homolog chain length, for alkyl esters, the sum of alkyl and acyl carbon numbers. Minor odd-numbered acid and alcohol homologs as well as even-numbered alkane homologs are omitted for clarity. Bars represent mean ± standard deviation (n = 4).

To provide complete reference data for ToF-SIMS peak assignment, the distributions of acyl and alkyl moieties within the wax esters were determined. Each of the aliphatic ester homologs represented a complex mixture of isomers derived from numerous pairwise combinations of acid and alcohol chain lengths. Since such metamers could not be chromatographically resolved and thus quantified by GC-FID, their distributions were determined instead based on abundances of characteristic fragments in the mixed mass spectrum associated with the GC peak of each ester homolog [23,31–35].

Three different patterns of isomer distributions could be discerned depending on overall ester homolog chain length, Fig. 5. In young *Phyllostachys aurea* leaves, the shorter ester homologs (C_{36}–C_{42}) were formed primarily by C_{20} alcohol and C_{16}–C_{22} acids, the mid-range esters (C_{42}–C_{44}) included a large portion of isomers formed by C_{26}–C_{28} alcohols and C_{16} acid, while the longer esters (C_{44}–C_{52}) contained mainly C_{22}–C_{30} alcohols and C_{22} acid. In the leaf wax mixtures of old leaves, similar patterns were found, with the C_{36}–C_{38} esters formed by C_{20} alcohol and C_{16}–C_{18} acids, the C_{40}–C_{44} esters by C_{24}–C_{28} alcohols and C_{16} acid, and the C_{46}–C_{52} esters by C_{24}–C_{30} alcohols and C_{22} acid. Overall, C_{22} acid was the most abundant acid in the linear VLC esters, independent of leaf age (compare Figs. 4B and 5A/C). The second-most abundant acid in alkyl esters was palmitic acid (C_{16}), most notably for old bamboo leaves (Figs. 4B and 5C).

Finally, the overall distribution of acid and alcohol moieties across all esters could be calculated, including alkyl esters and alicyclic (triterpenyl) esters. Thus, the chain length distribution of esterified acids was found to be bimodal, with maxima at C_{16} and C_{22} irrespective of plant age, Fig. 6A. The esterified acids had gradually decreasing abundances from C_{24} to C_{28}, in sharp contrast to the chain length profile of free acids gradually increasing towards C_{28} (compare Figs. 4A and 6A). The absolute amounts of individual esterified acid homologs were independent of leaf age, Fig. 6A.

In contrast to the profile of esterified acids, the chain length distribution of esterified alcohols differed between young and old

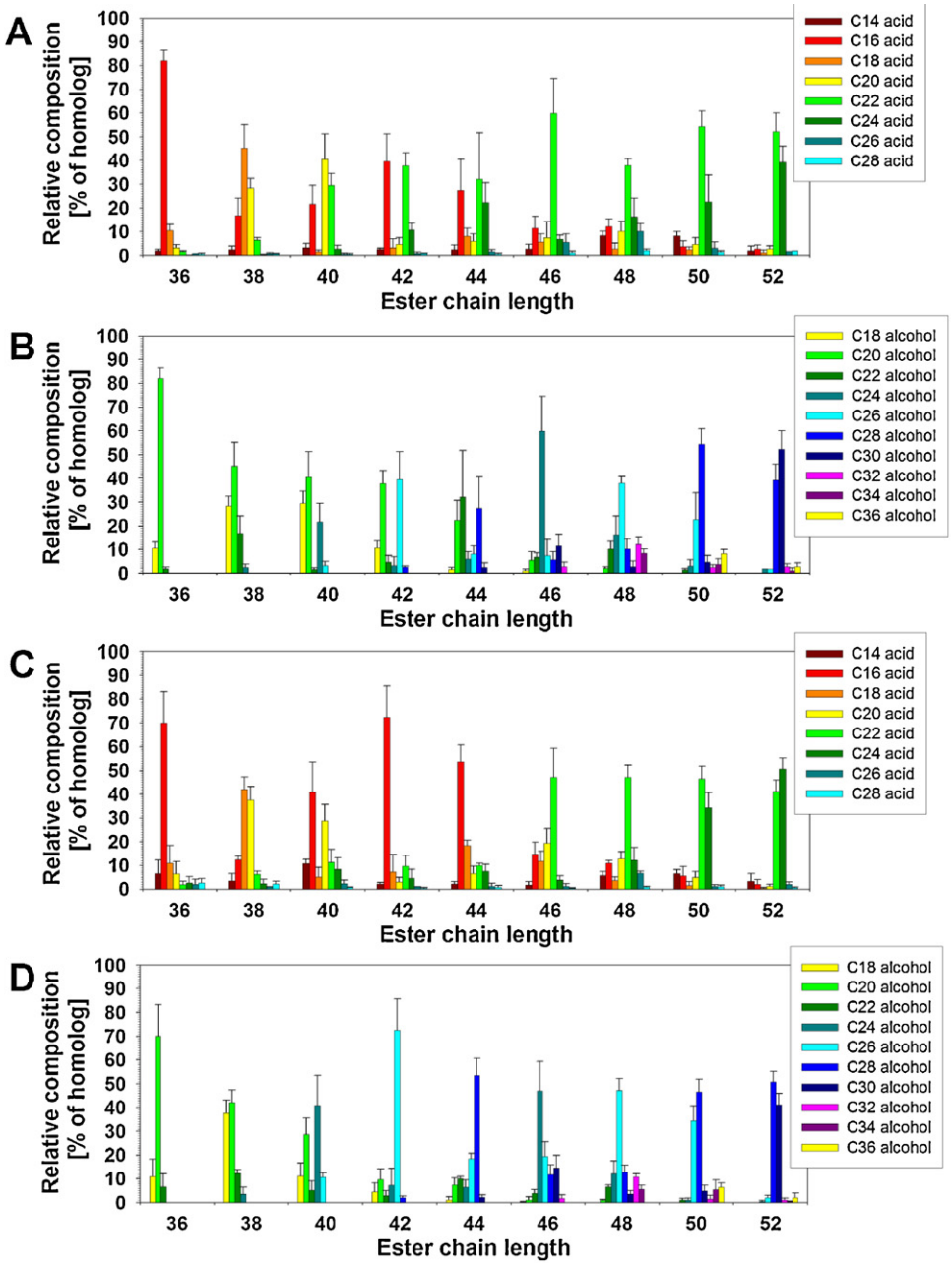

Fig. 5. Relative compositions of esterified acids and alcohols within the wax mixtures on the adaxial side of *Phyllostachys aurea* leaves. Relative abundances (%) of individual isomers are given by chain length of their acid moiety (A/C) and alcohol moiety (B/D) for each ester homolog, in young (A/B) and old (C/D) P. aurea leaves. Bars represent mean ± standard deviation (n = 4). Each group of bars adds up to 100%.

Table 2
XPS analysis of *Phyllostachys aurea* leaf surfaces. The elemental composition is averaged using data from three different positions at the margin and middle of two young and two old leaves – 24 sampled regions in total. In the case of silicon, which was not detected for all six analysis runs of each leaf region, the digit in brackets corresponds to the number of leaf samples which did show the presence of silicon. The —-$\underline{C_xH_y}$ hydrocarbon component at 285.0 eV is reported as a percentage of the overall C(1s) peak (set at 100%).

Phyllostachys aurea Adaxial Surface		Relative% Elemental Composition				
		C(1s)		O(1s)	N(1s)	Si(2p)
		C_{Total}	-$\underline{C_xH_y}$	O_{Total}	N_{Total}	Si_{Total}
Young	Margin	96.0 ± 0.7	82.6 ± 2.0	3.5 ± 0.6	0.5 ± 0.2	<0.1 ± 0.0 (3)
	Middle	93.7 ± 0.6	79.3 ± 3.3	5.4 ± 0.5	0.8 ± 0.1	0.2 ± 0.0 (5)
Old	Margin	84.0 ± 3.6	67.6 ± 3.1	12.0 ± 2.3	1.7 ± 0.4	2.3 ± 1.7 (6)
	Middle	84.4 ± 1.8	65.7 ± 2.2	12.4 ± 1.2	1.9 ± 0.4	1.4 ± 0.4 (6)

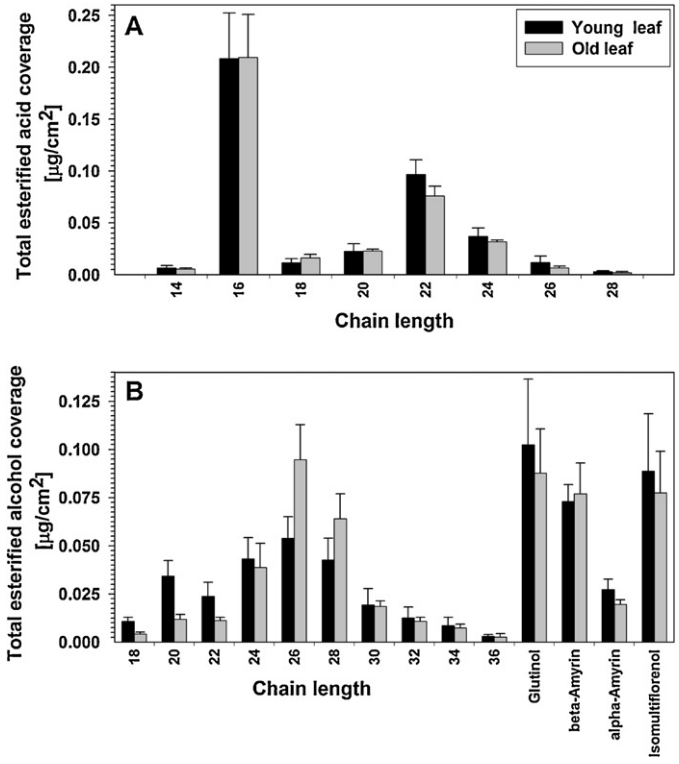

Fig. 6. Compositions of esterified acids and alcohols/triterpenols within the wax mixtures on adaxial side of *Phyllostachys aurea* leaves. Total coverages ($\mu g\,cm^{-2}$) of ester-bound acids (A) as well as alcohols and triterpenols (B) are given for young and old P. aurea leaves. Labels on the x-axis indicate either the chain length of esterified acids and alcohols, or the isomer name for triterpenols. Bars represent mean ± standard deviation (n = 4).

leaves. Higher levels of C_{18}–C_{22} alcohols were found in esterified wax of young *Phyllostachys aurea* leaves, and substantially more C_{26} alcohol in the wax esters of old leaves (Fig. 6B). The overall profile of esterified alcohols thus differed from that of corresponding free alcohol distributions, with the predominant chain length of C_{26} in the ester alcohols and C_{28} in the free alcohols (compare Figs. 4B and 6B). Similarly, the profiles of esterified and free triterpenols also differed (independent of age), most notably for glutinol (compare Figs. 4B and 6B).

3.4. Time-of-Flight secondary ion mass spectrometry (ToF-SIMS)

ToF-SIMS spectra of the leaf samples comprised peaks associated with whole and fragmented molecules (some of which were homologous series separated by 14/28 amu corresponding to differing numbers of CH_2/C_2H_4 units within alkyl chains), Fig. 7. Respective positive and negative ToF-SIMS spectra displayed different fragments at the margin of young leaves compared to the similar fragments detected for both the middle of young leaves and all across old leaves. The predominant species at the margin of young leaves were C_{22}-acid esters containing mainly C_{24}, C_{26}, and C_{28} esterified alcohols (based on GC–MS ester metamer analysis) together with very-long-chain C_{28}, C_{30}, and C_{32} amides. In contrast, towards the middle of young leaves and across the whole old leaves, there was a large proportion of the shorter chain C_{16} carboxylic acid in addition to free alcohols. This correlates well with the higher proportion of C16-C18 free acids observed for old leaves through GC analysis, Fig. 4B.

Imaging ToF-SIMS (using the stage raster mode) showed that the very-long-chain amide species were concentrated towards the margin region of young leaves, whilst the shorter C_{16} carboxylic acid was localised along the middle (axial centre) of the leaf, Fig. 8. In contrast, no such spatial distribution of the same species was observed for the case of the older leaves.

3.5. X-Ray photoelectron spectroscopy (XPS)

XPS survey spectra (0–1200 eV binding energy range) of margin/middle of young/old *Phyllostachys aurea* leaves detected the presence of the following main peaks: C(1s), O(1s), N(1s), Si(2p) and Si(2s). The percentage carbon content was highest overall in the young leaves, whilst the amount of oxygen and nitrogen was greatest in the old leaves, Table 2.

The high-resolution C(1s) envelope contained a main -$\underline{C}_xH_y$ hydrocarbon component at 285.0 eV (Supporting Information Fig. S 2). The C(1s) higher binding energy tail region comprised –$\underline{C}$-CX at 285.7 eV (where X represents: =O, (=O)NHR, –OOR, or –OOH) [36], –C–N at 286.0 eV, –$\underline{C}$–OH at 286.6 eV, $\underline{C}$=O/$\underline{C}$ONHR at 287.9 eV [37], and $\underline{C}$(=O)OR (where R is C or H), at 289.1 eV [36]. These values were consistent with those previously reported in the literature for leaf waxes of other species [38,39].

The O(1s) spectra were consistent with the C(1s) spectra, comprising complementary peak components: –$\underline{C}$ONHR at 531.6 eV, –C=$\underline{O}$ at 532.4 eV, –C–$\underline{O}$H at 533.1 eV, and –C(=O)$\underline{O}$R (where R is C or H) at 533.9 eV, (Supporting Information Fig. S 3) [36].

The N(1s) envelope consisted of two peaks at 400.2 eV and 401.7 eV, characteristic of amide (–C(=O)$\underline{N}$R) and protonated-amide ($-N^+HR_2$) functionalities, (Supporting Information Fig. S 3) [36,39,40]. The latter may also be associated with hydrogen-bonding between the amide nitrogen atom and nearby hydrogen-containing functional groups, such as alcohols [41,42]. The possibilities of N(1s) amine (–C–$\underline{N}H_2$) or nitrate functionalities were excluded because they typically appear below 400 eV [42,43] and around 407–408 eV, respectively. Nitrogen has been detected in XPS studies of other leaf surface waxes [39].

The Si(2p) spectra could be fitted with spin-orbit splitting components $\underline{Si}(2p_{3/2})O_2$ and $\underline{Si}(2p_{1/2})O_2$ at 103.3 eV and 103.9 eV respectively, corresponding to silica-like species (Supporting Information Fig. S 3) [36,44]. No peak was present at ~101.5 eV, ruling out polysiloxanes as a potential source of silicon contamination [45]. Previous XPS studies have identified silicon in leaf surface waxes, citing silica as one of its possible forms [39].

4. Discussion

In contrast to earlier studies, where differences in wax structure and chemistry have been noted between different plant species [46,47], or leaves on the same plant [48], sides of the same leaf [49], or stages of development [13,50], the dual wettability observed in the present study for young *Phyllostachys aurea* leaves appears to be a hitherto unreported wetting behaviour. This initial dual wettability displayed during the early stage of *P. aurea* leaf growth may ensure self-cleaning properties that prevent microbial growth and damage.

The mechanisms underpinning wetting comprise a chemical and physical component, Table 3. Assuming a wax density of $\approx 1\,g\,cm^{-3}$, the adaxial wax coverage measured by gas chromatography on young and old *Phyllostachys aurea* leaves ($3.6 \pm 0.4\,\mu g\,cm^{-2}$ and $3.3 \pm 0.1\,\mu g\,cm^{-2}$, respectively), corresponds to at least 30 nm effective wax layer thickness. The GC results provide a complete inventory of wax constituents, some or all of which may be present at the outermost surface. An important finding is the identification of C_{28}–C_{32} amides in both young and old leaves. Another is the detection of relatively high percentages of C_{22}-acid esters in young leaves and C_{16}–C_{18} free acids in wax of old leaves. These GC data have served as a reference for

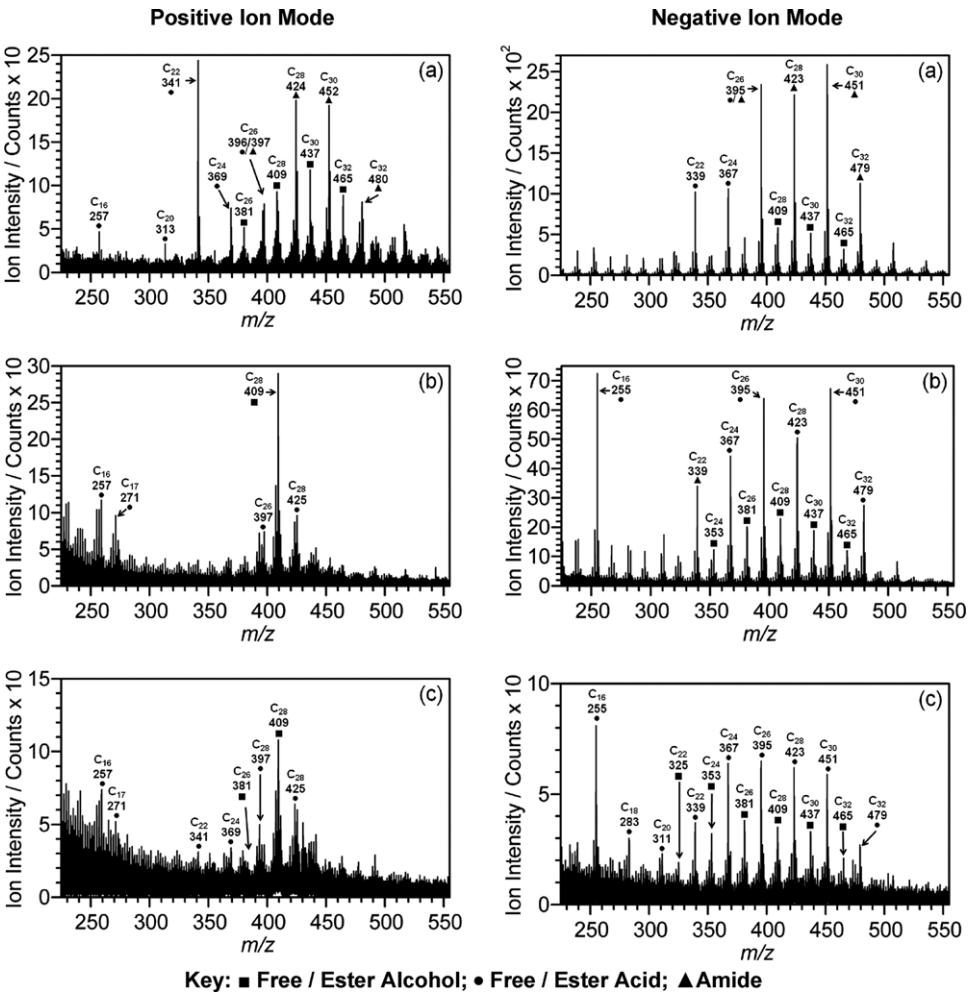

Fig. 7. ToF-SIMS of *Phyllostachys aurea* leaves showing predominant fragment assignments for: (a) the margin of a young leaf; (b) the middle of a young leaf; and (c) a raster scan across both the margin and middle of an old leaf.

Table 3
Summary of *Phyllostachys aurea* surface characteristics.

Technique	Young		Old
	Margin	Middle	All Over
Contact Angle	Hydrophobic	Hydrophilic	Hydrophilic
ToF-SIMS	More longer-chain species	More shorter-chain species	Uniform distribution of shorter-chain species
XPS	Predominantly hydrocarbon species	Higher level of oxygenated species	Higher level of oxygenated species
Electron Microscopy	Microscale papillae + Nanoscale wax platelets	Relatively small microscale papillae + Nanoscale wax granules	Poorly defined microscale papillae + Wax film

compound assignments in the corresponding XPS and ToF-SIMS datasets which provided highly surface-sensitive information with sampling depths comparable to contact angle analysis (wetting). XPS showed high carbon content on the adaxial surface of the young leaves, in accordance with the greater proportion of very long-chain aliphatic molecules, detected by GC, relative to old-leaf samples. The presence of oxygen and nitrogen XPS signals also agrees well with the GC assignments made for alcohols, carboxylic acids, esters, and amides. All of the imaging XPS data analyses correlated well with the corresponding ToF-SIMS results and ESEM images displaying dual wetting. Furthermore, imaging ToF-SIMS showed that longer- chain alkyl species with relatively low oxygen content dominate the young leaf margin region, whereas shorter-chain carboxylic acids and alcohols are found in greater relative concentrations towards the middle as well as throughout old leaves.

The longer hydrocarbon chains can help explain the greater hydrophobicity at the young leaf margin [51], however this alone cannot account for the very high (+140°) water contact angles observed. There also exists a contributing physical factor, attributed to the dense array of fine nanoscale epicuticular wax platelets found only in the margin regions of young leaves. The longer-chain species present towards the margin of young leaves, as shown by imaging ToF-SIMS, may have a strong tendency to form wax crystals due to their relatively narrow chain length distribution. These crystals may trap small air pockets, and thus facilitate the greater

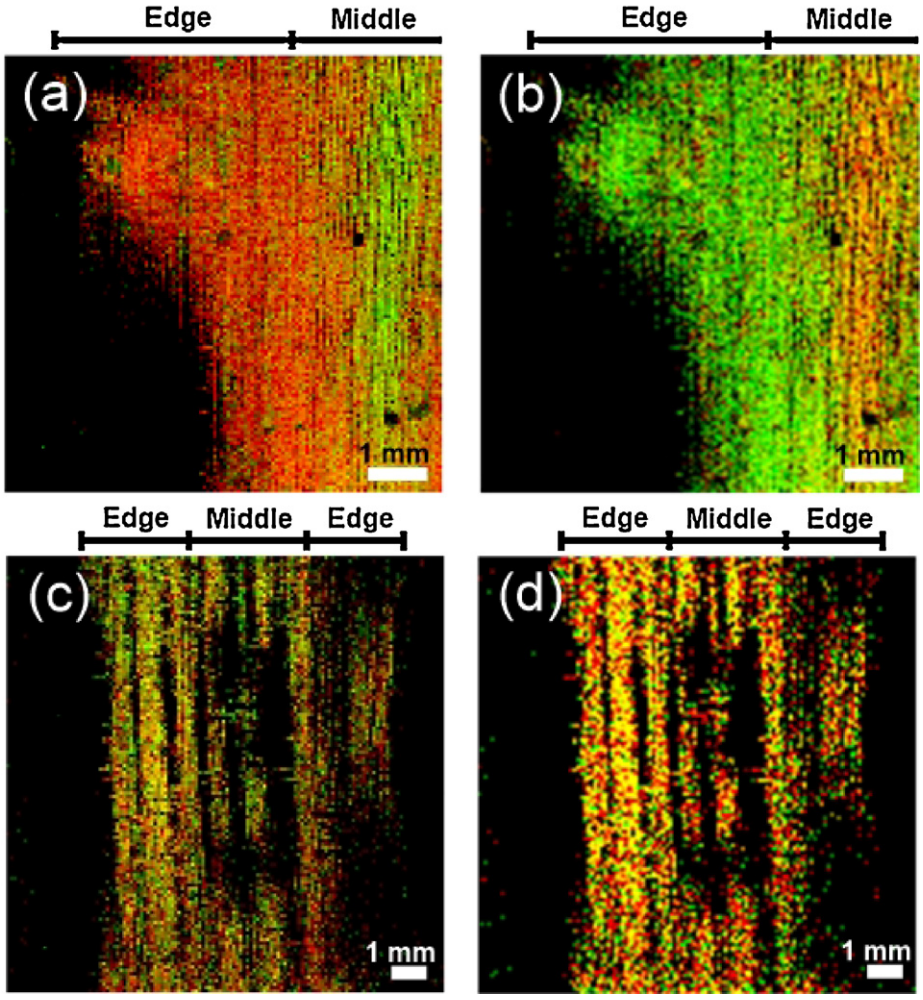

Fig. 8. Negative ion ToF-SIMS imaging of young (a–b) and old (c–d) *Phyllostachys aurea* leaves: (a)/(c) very-long-chain C_{30} amide ($m/z = -451$, red) versus long chain C_{22} free/esterified carboxylic acid ($m/z = -339$, green); and (b)/(d) C_{22} free/esterified carboxylic acid ($m/z = -339$, green) versus short chain C_{16} free/esterified carboxylic acid ($m/z = -255$, yellow) (for interpretation of the references to colour in this figure legend, the reader is referred to the web version of this article).

hydrophobicity and lower contact angle hysteresis associated with the Cassie-Baxter wetting state [4,52,53].

Given the inherent hydrophobicity of alkyl compounds found on the surface in the middle of young leaves, other factors must account for the observed hydrophilic nature in this region. This will include, the diminished surface roughness in the middle lowering hydrophobicity associated with the Cassie-Baxter wetting state. In the case of the older *Phyllostachys aurea* leaves, structural degradation or variation of the epicuticular wax chemical structure may be due to factors such as weathering (sunlight, wind, rain, etc.) eroding the surface over time [54,17]. Other possibilities include the much higher presence of silica on the surface of old leaves (detected by XPS, Table 2) perhaps being linked to both internal (plant) and external (environmental) sources. High levels of silica have been reported in *Phyllostachys* species [55,56]; including one study which found high concentrations of silica present in the epidermal walls [57]. However it is unclear as to whether transport of silica from the cell wall to the epicuticular wax occurs across the complex multi-layered structure of leaf cuticles [58]. The plentiful supply of silica in the earth's crust, might contribute to its presence on the leaf's surface through the attachment of particulates carried by wind, rain, insects, etc. Finally, the detection of a novel class of amides at the leaf surface is of interest; they may affect wax crystal formation and wettability, or moderate plant-herbivore and -pathogen interactions.

Given that it has been reported that dual wetting hydrophobic – hydrophilic arrays can yield much higher water collection efficiencies compared to straightforward hydrophobic or hydrophilic surfaces [59,60], the replication of *Phyllostachys aurea* bamboo dual wetting hydrophobic – hydrophilic channels surfaces may offer potential scope for fog collection and dew harvesting in water-scarce regions of the world [61]. The observed surface wetting behaviour of leaves may also have relevance to crop spraying.

5. Conclusions

The dual wettability behaviour displayed by young leaves of the *Phyllostachys aurea* bamboo can be attributed to a combination of the chemical and physical differences observed between the leaf margin and middle. The epicuticular nanoscale roughness combined with the very-long-chain alkyl compounds present in the margin regions of the leaves, gives rise to much higher water contact angles (droplet movement) compared to the middle of the leaves. These differences underpin the self-cleaning properties of the bamboo. Bioinspired replication of such dual wetting surfaces may have potential for water harvesting.

Data accessibility

Supporting data can be accessed at http://collections.durham.ac.uk.

Competing interests

We have no competing interests.

Author contributions

J.M.W., B.G.S., D.P.K.M., and D.J. assisted with plant identification; J.M.W., B.G.S., and J.P.S.B. assisted with contact angle analysis; J.M.W., B.G.S., and J.P.S.B. assisted with electron microscopy; J.M.W., R.C.R., M.T.H., I.W.F., R.J., and J.P.S.B. assisted with ToF-SIMS; R.C.R. and R.J. assisted with GC analysis; J.M.W., M.W., S.K.B., and J.P.S.B. assisted with XPS. All authors gave final approval for publication.

Funding

This work was supported by Engineering and Physical Sciences Research Council (EPSRC) grant reference EP/J005401/1.

Acknowledgements

We thank T. Davey of the Electron Microscopy Research Services at Newcastle University for the SEM imaging, P. Carrick of the Chemical and Materials Analysis Service at Newcastle University for the ESEM imaging, and NEXUS at Newcastle University for XPS analysis.

Appendix A. Supplementary data

Supplementary data associated with this article can be found, in the online version, at http://dx.doi.org/10.1016/j.colsurfa.2016.06.058.

References

[1] G. Eglinton, R.J. Hamilton, Leaf epicuticular waxes, Science 156 (1967) 1322–1335.
[2] P. Vukusic, J.R. Sambles, Photonic structures in biology, Nature 424 (2003) 852–855.
[3] A. Tuteja, W. Choi, M. Ma, J.M. Mabry, S.A. Mazzella, G.C. Rutledge, G.H. Mckinley, R.E. Cohen, Designing superoleophobic surfaces, Science 318 (2007) 1618–1622.
[4] W. Barthlott, C. Neinhuis, Purity of the sacred lotus, or escape from contamination in biological surfaces, Planta 202 (1997) 1–8.
[5] L. Feng, Y. Zhang, J. Xi, Y. Zhu, N. Wang, F. Xia, L. Jiang, Petal effect: a superhydrophobic state with high adhesive force, Langmuir 24 (2008) 4114–4119.
[6] H.G. Andrews, J.P.S. Badyal, Bioinspired hook surfaces based upon a ubiquitous weed (*Galium aparine*) for dry adhesion, J. Adhes. Sci. Technol. 28 (2014) 1243–1255.
[7] H.G. Andrews, E.A. Eccles, W.C.E. Schofield, J.P.S. Badyal, Three-dimensional hierarchical structures for fog harvesting, Langmuir 27 (2011) 3798–3802.
[8] R.M. von Spreckelsen, M.T. Harris, J.M. Wigzell, R.C. Fraser, A. Carletto, D.P.K. Mosquin, D. Justice, J.P.S. Badyal, Bioinspired breathable architecture for water harvesting, Sci. Rep. 5 (2015) 16798.
[9] M. Spaeth, W. Barthlott, Lotus-effect: biomimetic super-hydrophobic surfaces and their application, Adv. Sci. Technol. 60 (2008) 38–46.
[10] P.J. Holloway, Surface factors affecting the wetting of leaves, Pestic. Sci. 1 (1970) 156–163.
[11] B. Bhushan, Y.C. Jung, Micro- and nanoscale characterization of hydrophobic and hydrophilic leaf surfaces, Nanotechnology 17 (2006) 2758–2772.
[12] D.M. Hall, W. Burke, Wettability of leaves of a selection of New Zealand plants, New Zeal. J. Bot. 12 (1974) 283–298.
[13] R. Jetter, S. Schäffer, Chemical composition of the *Prunus laurocerasus* leaf surface: dynamic changes of the epicuticular wax film during leaf development, Plant Physiol. 126 (2001) 1725–1737.
[14] P.-G. Gülz, E. Müller, R.B.N. Prasad, Developmental and seasonal variations in the epicuticular waxes of *Tilia tomentosa* leaves, Phytochemistry 30 (1991) 769–773.
[15] A. Roth-Nebelsick, M. Ebner, T. Miranda, V. Gottschalk, D. Voigt, S. Gorb, T. Stegmaier, J. Sarsour, M. Linke, W. Konrad, Leaf surface structures enable the endemic Namib desert grass *Stipagrostis sabulicola* to irrigate itself with fog water, Interface 9 (2012) 1965–1974.
[16] K. Koch, W. Barthlott, Superhydrophobic and superhydrophilic plant surfaces: an inspiration for biomimetic materials, Phil. Trans. R. Soc. 367 (2009) 1487–1509.
[17] C. Neinhuis, W. Barthlott, Characterization and distribution of water-repellent, self-cleaning plant surfaces, Ann. Bot. 79 (1997) 667–677.
[18] Y. Yuan, T.R. Lee, Contact angle and wetting properties, in: G. Bracco, B. Holst (Eds.), Surface Science Techniques, Vol. 51, Springer, Berlin Heidelberg, 2013, pp. 3–34.
[19] R.E. Johnson Jr., R.H. Dettre, Wetting of low-Energy surfaces, in: J. Berg (Ed.), Wettability, Marcel Dekker, Inc., New York, 1993, Chapter 1, p 13.
[20] H.J. Ensikat, W. Barthlott, Liquid substitution: a versatile procedure for SEM specimen preparation of biological materials without drying or coating, J. Microsc. 172 (1993) 195–203.
[21] H.J. Ensikat, Liquid substitution methods, in: A.W. Robards, A.J. Wilson (Eds.), Procedures in Electron Microscopy, John Wiley & Sons, York, UK, 1996, pp. 66–76.
[22] M. Riederer, G. Schneider, Comparative study of the composition of waxes extracted from isolated leaf cuticles and from whole leaves of citrus: evidence for selective extraction, Physiol. Plant. 77 (1989) 373–384.
[23] C. Lai, L. Kunst, R. Jetter, Composition of alkyl esters in the cuticular wax on inflorescence stems from *Arabidopsis thaliana* cer mutants, Plant J. 50 (2007) 189–196.
[24] J. Schwieters, H.-G. Cramer, T. Heller, U. Jürgens, E. Niehuis, J. Zehnpfenning, A. Benninghoven, J. Vac. Sci. Technol. A 9 (1991) 2864.
[25] P.K. Ghosh, Spectra from solids and surfaces. introduction to photoelectron spectroscopy, in: P.J. Elving, J.D. Winefordner, I.M. Kolthoff (Eds.), Chemical Analysis: A Series of Monographs on Analytical Chemistry and Its Applications, John Wiley & Sons, New York, 1983, pp 161.
[26] C.D. Wagner, L.E. Davis, M.V. Zeller, J.A. Taylor, R.H. Raymond, L.H. Gale, Empirical atomic sensitivity factors for quantitative analysis by electron spectroscopy for chemical analysis, Surf. Interface Anal. 3 (1981) 211–225.
[27] J.F. Evans, J.H. Gibson, J.F. Moulder, J.S. Hammond, H. Goretzki, Angle resolved ESCA analysis of plasma modified polystyrene, Fresenius Z Anal. Chem. 319 (1984) 841–844.
[28] R.M. Friedman, J. Hudis, M.L. Perlman, Chemical effects on linewidths observed in photoelectron spectroscopy, Phys. Rev. Lett. 29 (1972) 692.
[29] G. Johansson, J. Hedman, A. Berndtsson, M. Klasson, R. Nilsson, Calibration of electron spectra, J. Electron Spectrosc. 2 (1973) 295–317.
[30] R.C. Racovita, R. Jetter, To be published.
[31] P.-G. Gulz, C. Markstädter, M. Riederer, Isomeric alkyl esters in *Quercus robur* leaf cuticular wax, Phytochemistry 35 (1994) 79–81.
[32] B. Reiter, M. Lechner, E. Lorbeer, R. Aichholz, Isolation and characterization of wax esters in fennel and caraway seed oils by SPE-GC, J. High Resolut. Chromatogr. 22 (1999) 514–520.
[33] T. Shepherd, G.W. Robertson, D.W. Griffiths, Compositional analysis of intact alkyl esters in leaf epicuticular wax of swede by capillary gas chromatography and electron-impact mass spectrometry, Phytochem. Anal. 6 (1995) 65–73.
[34] R.C. Racovita, C. Peng, T. Awakawa, I. Abe, R. Jetter, Very-long-chain 3-hydroxy fatty acids, 3-hydroxy fatty acid methyl esters and 2-alkanols from cuticular waxes of *Aloe arborescens* leaves, Phytochemistry 113 (2015) 183–194.
[35] F.M. Razeq, D.K. Kosma, O. Rowland, I. Molina, Extracellular lipids of *Camelina sativa*: characterization of chloroform-extractable waxes from aerial and subterranean surfaces, Phytochemistry 106 (2014) 188–196.
[36] G. Beamson, D. Briggs, High Resolution XPS of Organic Polymers, John Wiley & Sons Inc., New York, 1992, pp. 96–268.
[37] S.S. Jedlicka, J.L. Rickus, D.Y. Zemlyanov, Surface analysis by X-ray photoelectron spectroscopy of sol-gel silica modified with covalently bound peptides, J. Phys. Chem. B 111 (2007) 11850–11857.
[38] T. Hietala, N. Mozes, M.J. Genet, H. Rosenqvist, S. Laakso, Surface lipids and their distribution on willow (*Salix*) leaves: a combined chemical, morphological and physiochemical study, Colloids Surf. B 8 (1997) 205–215.
[39] M.C. Perkins, C.J. Roberts, D. Briggs, M.C. Davies, A. Friedmann, C.A. Hart, G.A. Bell, Surface morphology and chemistry of *Prunus laurocerasus* L. leaves: a study using X-ray photoelectron spectroscopy, time-of-flight secondary-ion mass spectrometry, atomic-force microscopy and scanning-electron microscopy, Planta 221 (2005) 123–124.
[40] A.E. Hooper, D. Werho, T. Hopson, O. Palmer, Evaluation of amine- and amide-terminated self-assembled monolayers as molecular glues for Au and SiO_2 substrates, Surf. Interface Anal. 31 (2001) 809–814.
[41] D. Wang, F.R. Jones, Surface analytical study of the interaction between (γ-amino propyl triethoxysilane and E-glass surface, J. Mater. Sci. 28 (1993) 2481–2488.
[42] N. Graf, E. Yegen, T. Gross, A. Lippitz, W. Weigel, S. Krakert, A. Terfort, W.E.S. Unger, XPS and NEXAFS studies of aliphatic and aromatic amine species on functionalized surfaces, Surf. Sci. 603 (2009) 2849–2860.
[43] J.E. Baio, T. Weidner, J. Brison, D.J. Graham, L.J. Gamble, D.G. Castner, Amine terminated SAMs: investigating why oxygen is present in these films, J. Electron. Spectrosc. Relat. Phenom. 172 (2009) 2–8.
[44] V.P. Zakaznova-Hezog, H.W. Nesbitt, G.M. Bancroft, J.S. Tse, X. Gao, W. Skinner, High-resolution valence-band XPS spectra of the non-conductors quartz and olivine, Phys. Rev. B 72 (2005) 205113.

[45] M. Ouyang, C. Yuan, R.J. Muisner, A. Boulares, J.T. Koberstein, Conversion of some siloxane polymers to silicon oxide by UV/Ozone photochemical processes, Chem. Mater. 12 (2000) 1591–1596.
[46] W. Barthlott, C. Neinhuis, D. Cutler, F. Ditsch, I. Meusel, I. Theisen, H. Wilhelmi, Classification and terminology of plant epicuticular waxes, Bot. J. Linn. Soc. 126 (1998) 237–260.
[47] C. Muller, M. Riederer, Plant surface properties in chemical ecology, J. Chem. Ecol. 31 (2005) 2621–2651.
[48] E. Stabentheiner, H.W. Pfeifhofer, J. Peters, M. Soledad Jiménez, Different surface characteristics or primary and secondary needles of *Pinus canariensis*, Flora 199 (2004) 90–99.
[49] F. Gniwotta, G. Vogg, V. Gartmann, T.L.W. Carver, M. Riederer, R. Jetter, What do microbes encounter at the plant surface? Chemical composition of pea leaf cuticular waxes, Plant Physiol. 139 (2005) 519–530.
[50] K. Bringe, C.F.A. Schumacher, M. Schimtz-Eiberger, U. Steiner, E.-C. Oerke, Ontogenic variation in chemical and physical characteristics of adaxial apple leaf surfaces, Phytochemistry 67 (2006) 161–170.
[51] K. Koch, H.-J. Ensikat, The hydrophobic coatings of plant surfaces: epicuticular wax crystals and their morphologies, crystallinity and molecular self-assembly, Micron 39 (2008) 759–772.
[52] A.B.D. Cassie, S. Baxter, Wettability of porous surfaces, Trans. Faraday Soc. 40 (1944) 546–561.
[53] A.B.D. Cassie, S. Baxter, Large contact angles of plant and animal surfaces, Nature 155 (1945) 21–22.
[54] E.A. Baker, G.M. Hunt, Erosion of waxes from leaf surfaces by simulated rain, New Phytol. 102 (1986) 161–173.
[55] P. Dayanandan, P.B. Kaufman, C.I. Franklin, Detection of silica in plants, Am. J. Bot. 70 (1983) 1079–1084.
[56] H. Motomura, K. Hikosaka, M. Suzuki, Relationships between photosynthetic activity and silica accumulation with ages of leaf in *Sasa veitchii* (Poaceae, bambusoideae), Ann. Bot. 101 (2008) 463–468.
[57] A. Lux, M. Luxova, J. Abe, S. Morita, S. Inanaga, Silification of bamboo (*Phyllostachys heterocycla* Mitf.) root and leaf, Plant Soil 85 (2003) 85–91.
[58] K. Koch, B. Bhushan, W. Barthlott, Diversity of structure, morphology and wetting of plant surfaces, Soft Matter 4 (2008) 1943–1963.
[59] R.P. Garrod, L.G. Harris, W.C.E. Schofield, J. McGettrick, L.J. Ward, D.O.H. Teare, J.P.S. Badyal, Mimicking a *Stenocara* beetle's back for microcondensation using plasmachemical patterned superhydrophobic-superhydrophilic surfaces, Langmuir 23 (2007) 689–693.
[60] A.R. Parker, C.R. Lawrence, Water capture by a desert beetle, Nature 414 (2001) 33–34.
[61] The United Nations World Water Development Report 4: Managing Water under Uncertainty and Risk; UNESCO, Paris, 2012; p 79.